Extreme Mechanics Letters 40 (2020) 100946

Contents lists available at ScienceDirect

Extreme Mechanics Letters

journal homepage: www.elsevier.com/locate/eml

Atomistic mechanism of stress modulated phase transition in monolayer $MoTe_2$

Arman Ghasemi, Wei Gao *

Department of Mechanical Engineering, University of Texas at San Antonio, San Antonio, TX 78249, USA

ARTICLE INFO

Article history:
Received 3 May 2020
Received in revised form 13 July 2020
Accepted 11 August 2020
Available online 20 August 2020

Keywords:
2D materials
Transition metal dichalcogenides (TMD)
$MoTe_2$
Phase transition
Nudged elastic band method
Density functional theory

ABSTRACT

Monolayer $MoTe_2$, one of the 2D transition metal dichalcogenide (TMD) materials, exhibits two stable structural phases: semiconducting 2H phase and metallic 1T′ phase. The dynamic control of the transition between these two phases on a single atomically thin sheet holds promise for a variety of revolutionary device applications. Particularity, stress could be utilized to dynamically modulate such phase transition. To date, the atomistic and kinetic mechanism of the phase transition under stress is not clear. In this paper, the finite deformation nudged elastic band method and density functional theory are applied to determine the phase transition barriers and pathways of monolayer $MoTe_2$ as a function of applied stress. It is found that the stress can greatly influence the thermodynamics and kinetics of the phase nucleation and propagation. The results shed light on the phase engineering of 2D TMD materials with stress at the atomic level.

1. Introduction

Monolayer group-VI transition metal dichalcogenide (TMD) materials have multiple crystal phases with different physical properties. The generalized formula of these TMD materials is MX_2, where M represents a transition metal (Mo or W) in group-VI and X represents a chalcogen (S, Se or Te). These 2D materials have recently shown great promise for phase engineering applications at the atomically thin limits, which can lead to revolutionary devices such as memory devices [1], reconfigurable circuits [2] and topological transistors [3]. Monolayer $MoTe_2$ is one of the members inside this 2D material family. One of the stable phases of monolayer $MoTe_2$ is 2H, as shown in Fig. 1, the monolayer is composed of a layer of hexagonally arranged transition-metal atoms (blue color), sandwiched between two layers of chalcogen atoms (orange and yellow colors). Monolayers of $MoTe_2$ in 2H phase are semiconductors with a direct band gap. A hexagonal 1T phase is generated by shifting one of the Te layers around Mo atoms. This 1T structure is energetically unstable, so it turns into conducting 1T′ phase with monoclinic symmetry. Inside the 2D TMD family, $MoTe_2$ has the least energy difference between 2H and 1T′ at the ground state [4], thus it exhibits great potential for phase engineering applications [5,6].

One of the fascinating properties of 2D materials is their high stretchability and possibility to use external deformation to manipulate their physical properties in a controlled manner [7–9]. A recent experiment showed that nanoindentation applied by Atomic Force Microscope can induce phase transition on $MoTe_2$ thin films at ambient condition [5]. In addition, the phase transition of monolayer MoS_2 and $MoTe_2$ has been experimentally reported through chemical/thermal doping [10,11], laser patterning [12] and electrostatic gating [6]. In these phase engineering processes, stress could play an important role, for example, by thermal stress, and the stress induced by lattice mismatches and interactions with substrates. Meanwhile, combining the stress modulation with other phase engineering approaches could potentially lead to more versatile phase controls. With current nanomechanical techniques, stress can be applied to 2D materials through micromechanical device [13], nanoindentation [5,14,15], blister pressure [16–19], interfacial load transfer [20,21], thermal expansion [22] and so on.

On the theoretical sides, Reed and co-workers [4] calculated the energies of various 2D TMDs at different phases under strains and conducted a thermodynamics analysis, from which they suggested the promising application of mechanical deformation to the phase engineering of these materials. Following their work, the simulations with nudged elastic band (NEB) method demonstrated the kinetics of the phase transition under the applied strains [23–25]. However, there are two limitations of previous studies. First, due to the limitation of conventional NEB method, all these calculations were conducted at fixed geometry, where the lattice is unable to deform during the calculations of transition pathway. While in reality, lattices are allowed to change geometries during phase transition. Recently, we developed a

* Corresponding author.
E-mail address: wei.gao@utsa.edu (W. Gao).

https://doi.org/10.1016/j.eml.2020.100946
2352-4316/

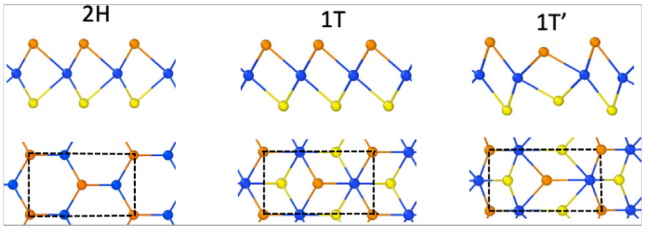

Fig. 1. Cross-sectional and basal plane views of 2D $MoTe_2$ crystal structure at different phases. Blue color: Mo; orange/yellow color: Te atoms on the top and bottom layers. The dashed lines represent the unit cells of the crystals. (For interpretation of the references to color in this figure legend, the reader is referred to the web version of this article.)

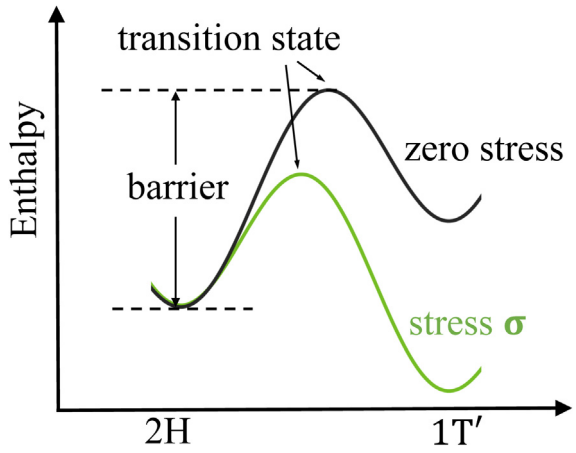

Fig. 2. Schematic demonstration of the stress dependent minimum energy path (MEP) for phase transition between 2H and 1T′ phases of $MoTe_2$.

finite deformation nudged elastic band (FD-NEB) method [26], which uses applied stress as the control variable instead of strain, so finite lattice deformations can be considered during the search of transition pathways. Second, previous phase transition calculations [23–25,27] only studied the concerted transition, where all the atoms transform to the new phase simultaneously. While in reality, phase transition could nucleate from a localized site, followed by the propagation of the new phase. These phase nucleation and propagation processes are studied in this paper with FD-NEB method. In addition to the studies at the atomic scale, the phase transition of TMD materials has been studied with phase field method at the mesoscale [28].

The mechanism of the phase transition of $MoTe_2$ can be schematically described by Fig. 2, where the horizontal and vertical coordinates respectively represent the structure evolution and the energy variations during phase transition process. Under an external stress, the energy landscape can be generalized to a static enthalpy landscape in order to include the work done by the applied stress. The double-well curve represents the most probable phase transition pathway, i.e. minimum energy path (MEP). To have a phase transition from 2H to 1T′, the material needs to across a transition state at the peak of MEP, overcoming a barrier $\Pi^{\neq}$. According to transition state theory [29,30], this barrier determines phase transition rate, described by $k(\boldsymbol{\sigma}) \propto \exp\left[-\Pi^{\neq}(\boldsymbol{\sigma})/k_B T\right]$, where k is transition rate, k_B is Boltzmann constant and T is temperature. The lower the barrier, the higher the rate and more likely transition occurs. At the ground state (zero stress), 2H phase is a more stable phase with a lower potential energy. When a stress $\boldsymbol{\sigma}$ is applied, 1T′ phase could become more thermodynamically favorable. Additionally, from the kinetics point of view, the phase transition from 2H to 1T′ occurs when the barrier $\Pi^{\neq}$ can be overcome by the external energetic excitation. The stress $\boldsymbol{\sigma}$ shown in Fig. 2 reduces this barrier, thereby facilitating the transition from 2H to 1T′. The phase transition barriers and MEPs can be calculated as a function of applied stress field with FD-NEB method [26]. Meanwhile, it is also possible to analytically estimate the stress dependent barriers with recently developed finite deformation Bell theory [27]. In this paper, FD-NEB method is applied to calculate the barriers and MEPs of phase nucleation and propagation with the aim to understand both of the thermodynamics and kinetics of the phase transition at the atomic scale.

2. Computation method

Phase transition pathways and barriers can be calculated with transition state methods such as nudged elastic band (NEB) method. The conventional NEB [31] only takes atomic positions as transition variables. However, for the phase transitions of solid materials under stress, the lattice deformation also contributes to the search of MEP, so it also needs to be explicitly added to the transition variables in addition to the atom positions. Recently, a finite deformation NEB (FD-NEB) method [26] was formulated by adding finite deformation variables to previous solid-state NEB method [32]. In a FD-NEB calculation, a band (which represents transition path) is initially constructed by connecting a number of intermediate states between the given initial and final states (which are subjected to the same stress). These intermediate states are generated by a geometric interpolation between the initial and final states as an initial guess. The purpose of FD-NEB algorithm is to move the band until it converges to the MEP under a given stress. FD-NEB has been implemented based on the Atomic Simulation Environment (ASE), an open source Python package for setting up and steering atomistic simulations, which provides an interface to various external atomistic computational codes, such as VASP and LAMMPS.

In FD-NEB simulations, the energies, forces and stress can be computed by either empirical atomic potentials or more accurate Density Functional Theory (DFT). So far, there is no reliable empirical atomic potential that can properly describe the phase transition of $MoTe_2$, hence DFT is chosen as the calculator for FD-NEB simulations. All the DFT calculations in this study are performed using the plane-wave-based VASP [33,34]. Electron exchange and correlation energies are calculated with the generalized gradient approximation using the Perdew–Burke–Ernzerhof (PBE) functional [35]. The projector augmented wave (PAW) method [36,37] is used to represent ionic cores. The kinetic energy cutoff for the plane-wave basis describing the valence electrons is set to 292 eV, and the k-point used to sample Brillouin zones of the supercell are $1 \times 5 \times 1$. In order to validate the k-point convergence, we have also conducted a few calculations up to $7 \times 9 \times 1$ k-point, which yield almost the same barriers and transition paths as $1 \times 5 \times 1$ k-point. A vacuum layer of thickness 3 nm is used to prevent the van der Waals interactions between periodic images of $MoTe_2$ sheet.

3. Phase transition at zero stress

Fig. 3 shows the transition process of a supercell composed by 3 $MoTe_2$ unit cells arranged along armchair direction. To identify the phase nucleation process in FD-NEB calculation, the following method is applied: whenever an intermediate stable state (indicated by a local minimum in MEP) is observed in MEP search, it is taken out for another new NEB calculation (which uses this state as a new final state). This procedure is repeated until no local minimum is found on MEP, so that the nucleated state is directly connected to the original state by a single barrier.

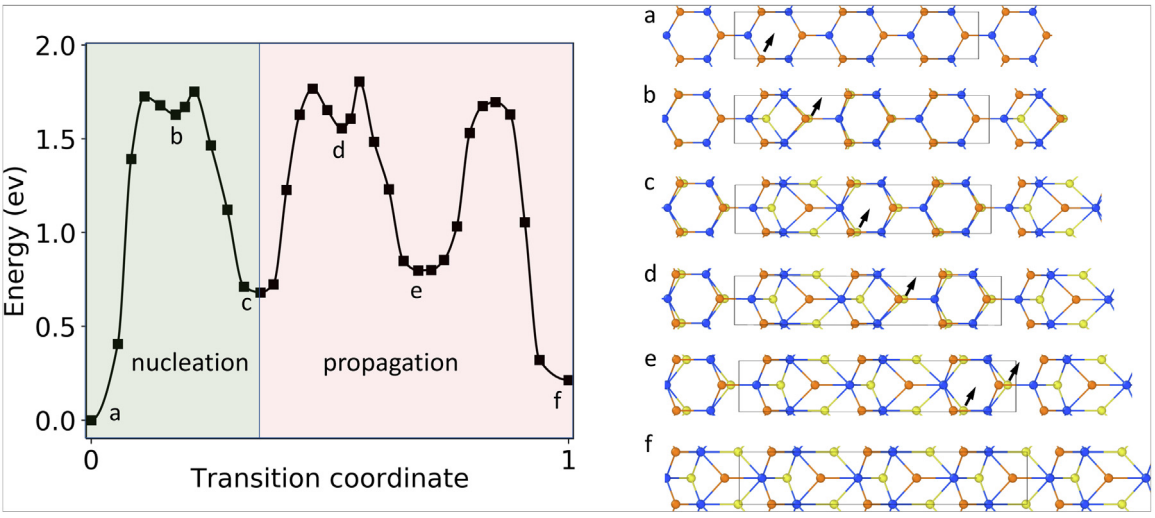

Fig. 3. The MEP of the phase transition between 2H and 1T′ under zero stress, including the nucleation inside one unit cell ($a \rightarrow c$) and the propagation to the neighboring cells ($c \rightarrow f$). The atomic structures corresponding to the local minima are plotted to demonstrate the variation of the atoms and the supercell during the transition, where the box represents the supercell with periodic boundary condition and the arrows indicate the movements of Te atoms (yellow color). (For interpretation of the references to color in this figure legend, the reader is referred to the web version of this article.)

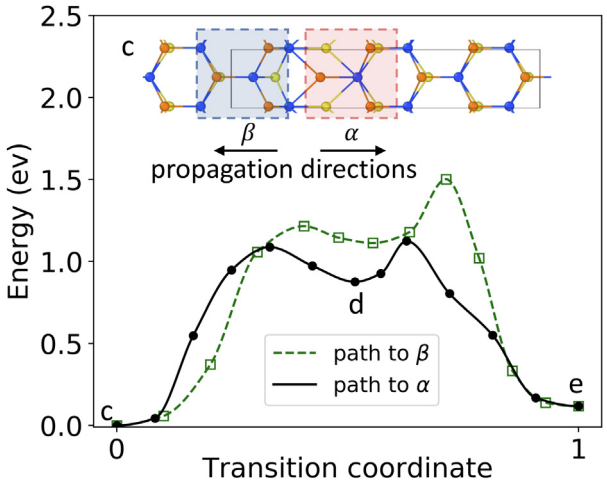

Fig. 4. Comparison of two possible pathways for the phase propagation. The barrier of the path to the α phase boundary (solid black line) is lower, so the propagation to the right is more kinetically favorable. Note that the path to α is the same as the c→d→e curve in Fig. 3, but with a shift of the reference energy.

The same approach is also applied to identify the pathway of propagation. Finally, the MEP obtained with this approach shows a series of barriers and minima along the path.

As shown in Fig. 3a, 1T′ phase nucleates from the unit cell on the left, where one of the Te atoms in the bottom layer (yellow color) shifts out toward the center of 2H hexagon; meanwhile the neighboring atoms are slightly shifted from their original positions. Across a metastable transition state, a local minimum appears on the MEP, which corresponds to a stable intermediate phase shown in Fig. 3b. Sequentially, another Te atom in the bottom layer moves out by overcoming another small barrier to complete the nucleation process. At the end, a unit cell with 2H phase is completely transformed to 1T′ phase, as shown in Fig. 3c.

After the nucleation, two phase boundaries represented by α and β in Fig. 4, are formed on each side of the transformed 1T′ cell. The phase propagation may follow two possible directions, respectively towards α or β phase boundary. The NEB calculations indicate that the path to α is more kinetically favorable since it corresponds to a lower propagation energy barrier, as shown in Fig. 4. During the first propagation ($c \rightarrow e$), the atoms experience similar sequential movement as observed in nucleation. However, during the second propagation (e→f), two Te atoms move simultaneously, which is most likely due to the different confinement on the unit cells. As a result, no local minimum appears on the MEP. If there are more unit cells added along armchair direction, it is expected that a similar propagation process would continue in a one-cell-by-one-cell fashion.

It is noted that the process shown in Fig. 3 is still concerted on zigzag direction due to periodic boundary conditions, meaning that all the atoms along zigzag direction have to move simultaneously during the phase transition. This kind of transition is applicable to a nanoribbon where the nucleus is able to extend across the sheet on zigzag direction. Additionally, a recent experiment [6] has shown a concerted atomic motion along zigzag direction during the phase transition of monolayer $MoTe_2$ sheet activated by the electrostatic gating inside the ionic liquid. In this experiment, the authors reported that "it is energetically favorable for the zigzag axis to be maintained during phase transition through intralayer atomic plane gliding" and "such orientation locking occurs on a much larger scale (about 10 μm^2)". To investigate the possible nucleation along zigzag direction, we conducted NEB calculations on a supercell composed by several unit cells arranged along zigzag direction. It is found that all the unit cells transform simultaneously without forming a phase boundary. This implies that the phase boundary along armchair direction may have a high interface energy. As a result, in a relatively small supercell, the barrier for nucleation would be even higher than the barrier of concerted transition, thereby the concerted nucleation is preferred. If the computation power allows, one could use a larger supercell to study the nucleation on zigzag direction, which may occur with the simultaneous nucleation of a number of unit cells, instead of the nucleation of one unit cell as shown along armchair direction. It is noted that DFT is too computationally expensive to conduct such NEB calculations with a large supercell, so a reliable empirical potential that can properly describe the phase transition will be needed.

4. Stress modulated phase transition

In this paper, the phase transition of $MoTe_2$ is studied under tensile stress that is applied on armchair or zigzag direction.

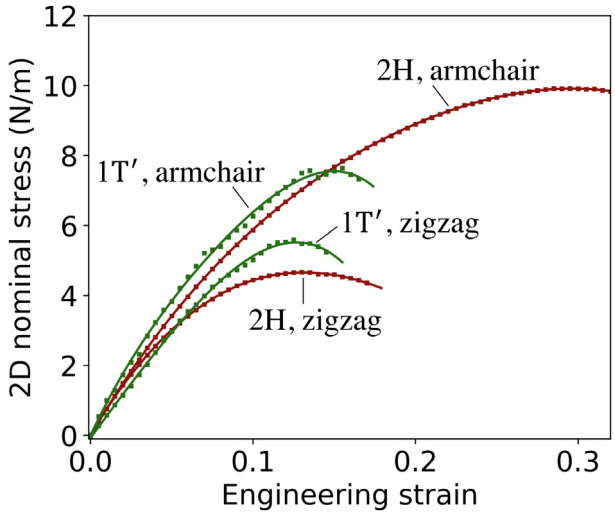

Fig. 5. Stress–strain relationships of monolayer $MoTe_2$ at 2H and 1T′ phases stretched uniaxially on armchair and zigzag directions. The solid curves are fourth order polynomial fits.

Like other 2D materials, $MoTe_2$ exhibits hyperelastic behavior under finite deformation. Fig. 5 shows the stress–strain curves of monolayer $MoTe_2$ obtained from molecular statics simulations, in which the 2D sheet is uniaxially stretched on armchair or zigzag direction while relaxing the stress on the other direction. The 1T′ monoclinic crystal with two-fold symmetry shows more significant anisotropic behavior even at small strain as compared with 2H hexagonal crystal with six-fold symmetry. Along armchair direction, the ultimate athermal stress of 1T′ phase is 7.6 N/m, therefore the range of stress used in the study is 0–6 N/m. Likewise, the range of stress applied on zigzag direction is 0–4 N/m, since the ultimate athermal stress of 2H phase along zigzag direction is 5.6 N/m. It should be noted that the phase transition does not occur by stretching the sheet when there is no thermal activation. By contrast, athermal loading can lead to phase transition in some phase change materials such as silicon in which the transition is induced by lattice instability [26,38]. It is also not expected to see phase transition of $MoTe_2$ in molecular dynamics simulation due to the limitation on the accessible simulation time scale. Therefore, FD-NEB method [26], as an indirect approach, is applied here to search the phase transition pathways in the high dimensional enthalpy landscape.

In general, when subjected to a nominal stress tensor $\boldsymbol{\sigma}$, the enthalpy barrier is calculated as [26]

$$\Pi^{\neq}(\boldsymbol{\sigma}) = \mathcal{V}^{\neq}(\boldsymbol{\sigma}) - V_0\boldsymbol{\sigma} : (\mathbf{F}^{(t)} - \mathbf{F}^{(o)}), \tag{1}$$

where $\mathcal{V}^{\neq}$ is the potential energy difference between transition and initial state, $\mathbf{F}^{(t)}$ and $\mathbf{F}^{(o)}$ are respectively the deformation gradients of the transition and initial state under stress $\boldsymbol{\sigma}$ with respect to the reference state (whose volume is V_0). While there are no restrictions on choosing the reference state, for convenience, we select the initial 2H phase under zero stress as the reference state in FD-NEB calculations. For the uniaxial tensions, Eq. (1) can be simplified as

$$\Pi^{\neq}(\sigma) = \mathcal{V}^{\neq}(\sigma) - A_0\sigma(\lambda^{(t)} - \lambda^{(o)}), \tag{2}$$

where σ is the 2D uniaxial nominal stress (unit: N/m) and λ is the stretch on the loading direction. Fig. 6 shows that the nucleation barrier decreases as the increase of stress applied on armchair direction (σ_x) but slightly increase when the stress is applied on zigzag direction (σ_y). A sudden drop of the nucleation barrier is shown in Fig. 6b at 2 N/m, which implies a change of the transition mechanism. To understand this, we calculated the engineering strain of the transition state with respect to the initial state, which is plotted as the parallel y-axis in Fig. 6b. Interestingly, the strain exhibits a sudden increase at 2 N/m. This indicates that the phase nucleation becomes more dominated by the deformation of the supercell beyond 2 N/m. While below this stress, the nucleation is more dominated by the atomic motions. Nevertheless, it is found that the atom movements during the nucleation under stress is very similar to that at zero stress as shown in Fig. 3.

From Fig. 6a, it can be noted that the enthalpy of the nucleated phase is greater than that of the initial phase even at $\sigma = 6$ N/m, meaning that this kind of nucleation is not thermodynamically favorable. It further implies that the nucleation may involve several unit cells that simultaneously transform along armchair direction rather than a single cell nucleation. Given N initial 2H unit cells in the supercell, if M cells transform from 2H to 1T′ simultaneously during the nucleation, the enthalpy of the initial and nucleated structures are respectively $N\pi_H(\sigma)$ and $(N-M)\pi_H(\sigma)+M\pi_T(\sigma)+E_b(\sigma)t$, where π_H, π_T are the enthalpy of 2H and 1T′ unit cell, E_b is the phase boundary energy per unit length, and t is the thickness of the phase boundary. Then, the difference of enthalpy between the initial and nucleated structure is $\Delta\Pi(\sigma) = M[\pi_H(\sigma) - \pi_T(\sigma)] - E_b(\sigma)t$. When $\Delta\Pi(\sigma) \geq 0$, the nucleated phase becomes thermodynamically favorable. Hence, the minimum number of cell nucleated simultaneously can be calculated as

$$M = \frac{E_b(\sigma)t}{\pi_H(\sigma) - \pi_T(\sigma)}. \tag{3}$$

As shown in Fig. 7, when $\sigma_x < 2N/m$, $\pi_H < \pi_T$, so the nucleation of 1T′ in this case is always not thermodynamically favorable, while π_H becomes greater than π_T as σ_x increases. The phase boundary energy E_b can be calculated by $[\Pi^{o}(\sigma) - \Pi^{n}(\sigma)]/t$, where Π^{o} is the enthalpy of the supercell with all 2H unit cells, and Π^{n} is the enthalpy of the supercell after the nucleation when some of 2H unit cells are transformed to 1T′ phase. It is noted that E_b is the combination of the interface energies of two phase boundaries, α and β. Using Eq. (3), the calculated values of M are shown in Fig. 7b. A minimum number of 4, 8 and 35 unit cells are required to nucleate simultaneously under 6, 4 and 2 N/m tensile stress, so that the nucleated structures become thermodynamically favorable. It is expected that the kinetics of the nucleation of multiple cells as well as their atomic motions during the transition are similar to those observed in single unit cell nucleation.

It should be noted that only the effects of stress are considered in the above thermodynamics analysis of nucleation. In phase engineering applications, there are other approaches can be used to tune the thermodynamics. For example, electrostatic gating [6,39] has been shown theoretically and experimentally as an effective way to modulate the thermodynamic relationship between 2H and 1T′ phases. However, the kinetics of the phase nucleation under electrostatic gating is still not clear. This could be studied by adding electrostatic charges into NEB calculation in the future. Moreover, it was found in previous studies that shear stress could largely influence material's phase transition behavior [40–42], so it will be of great interest to further investigate the effect of shear stress in 2D materials on their phase transition behavior.

Next, we discuss the stress modulated phase propagation. As shown in Fig. 8a, the MEP shapes are similar to the case of zero stress, while the barrier decreases with σ_x and slightly increases with σ_y. Since the phase propagation does not create a new phase boundary, it is always thermodynamically favorable, as long as $\sigma_x > 2$ N/m when the newly formed 1T′ phase stays at a lower enthalpy as compared with 2H phase. Interestingly, it is

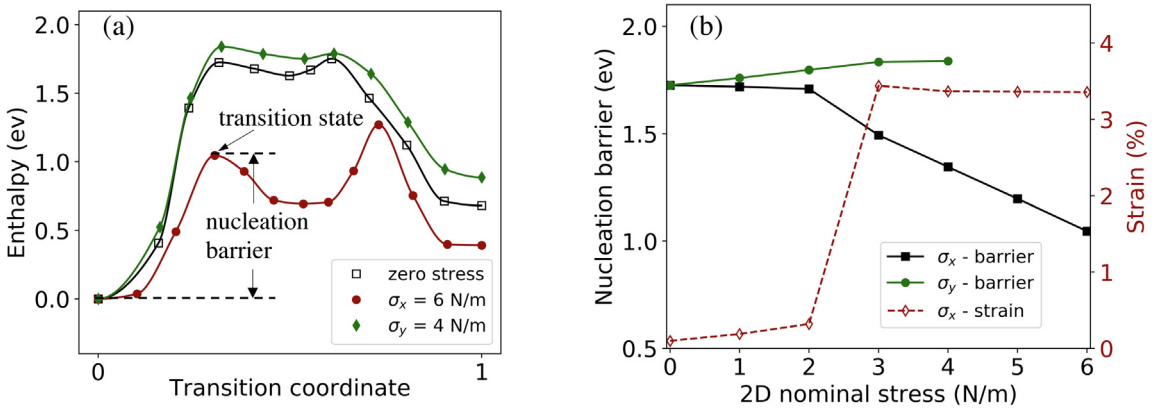

Fig. 6. (a) Comparison of the MEPs of phase nucleation under different stresses. The peak points in MEP correspond to the transition states of phase nucleation and propagation. (b) The left y axis shows the nucleation barrier as a function of applied stress. The right y axis represents the deformation between 2H phase and the transition states under the stress applied on armchair direction.

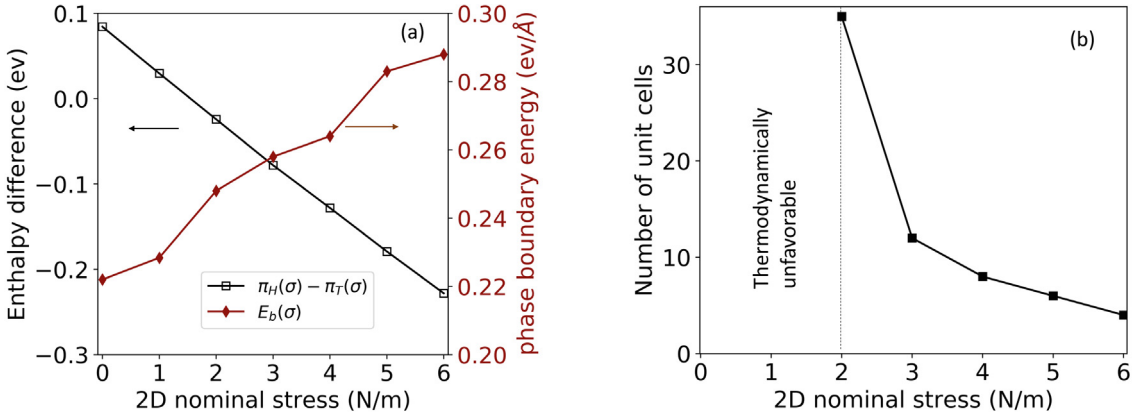

Fig. 7. (a) The enthalpy difference between 2H and 1T′ unit cell and the phase boundary energy as a function of applied stress along armchair direction. (b) The minimum number of unit cells that are nucleated simultaneously to ensure the nucleated structure is thermodynamically favorable.

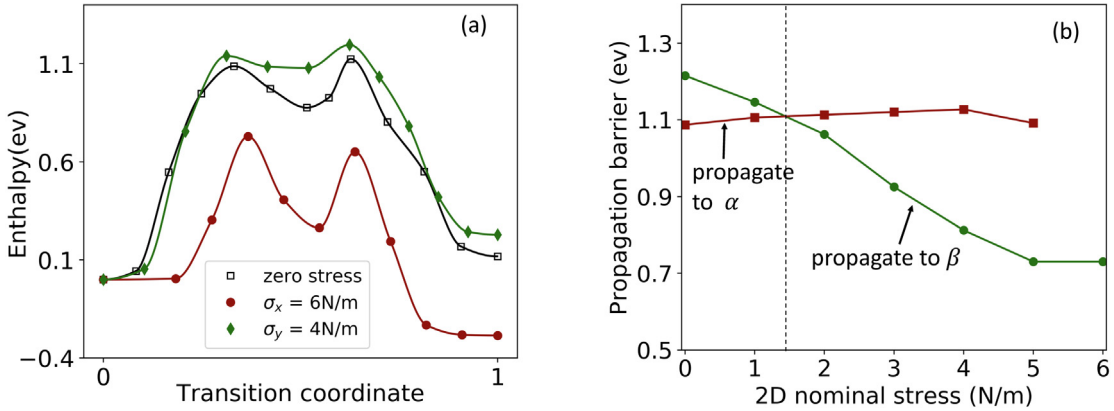

Fig. 8. (a) The MEPs of phase propagation at different stresses. (b) Comparison of two possible propagation directions as a function of the applied stress on armchair direction. The propagation to the β phase boundary becomes kinetically favorable beyond 1 N/m.

found that the propagation towards β phase boundary becomes more kinetically favorable (with lower propagation barrier) when $\sigma_x > 1$ N/m, which suggests a useful way to modulate the phase propagation with stress. By contrast, when the stress is applied on zigzag direction, the preferred propagation direction is always towards α phase boundary.

Based on the simulation results calculated with the supercell, the lower bounds of the nucleation and propagation barriers are respectively around 1 eV and 0.7 ev when $\sigma_x = 6$ N/m. These values have to be further multiplied by the number of unit cells that are transformed simultaneously along zigzag direction, in order to get the transition barriers in a real pristine $MoTe_2$. Unfortunately, the nucleation on the zigzag direction is to be studied in the future as discussed above, so the exact value of the transition barriers in a pristine crystal is not determinable in this study. Generally, a barrier around 0.6 eV can be overcome by room temperature thermal fluctuation at experimental time scale based on the transition state theory. Therefore, our current calculations imply that the phase transition of a pristine $MoTe_2$ is not kinetically favorable under room temperature. In another word,

it is not likely to have the phase transition occurring in a pristine crystal at room temperature even under a large stress. However, a recent experiment reported a phase transition in $MoTe_2$ thin films induced by mechanical deformations [5]. If this experiment is reliable, it indicates that the material defects inside $MoTe_2$ must play important roles in phase transition. One important feature of synthesized $MoTe_2$ is that they are generally divided into many small grains by grain boundaries [43,44]. In addition, point defects such as vacancies and antisites have been observed in $MoTe_2$ [45,46]. These defects could help to reduce the barriers; meanwhile, due to lattice mismatches, these defects can also produce significant stress concentration around nearby regions, facilitating the phase nucleation. It is not realistic to study the effects of sophisticated defects with DFT based NEB calculations. Instead, a properly calibrated empirical atomic potential will be needed. Finally, despite that applying stress alone may not be able to achieve phase transition in a pristine $MoTe_2$, stress can be combined with other phase engineering approaches to modulate the thermodynamics and kinetics of the transition, as shown in this study.

5. Conclusion

Stress plays important role in the phase transition of monolayer $MoTe_2$ and can be utilized as a useful tool in the phase engineering applications. In this paper, the transition barriers and pathways of a pristine $MoTe_2$ are calculated by using finite deformation nudged elastic band method and density functional theory. The kinetic and thermodynamic analysis are conducted for both phase nucleation and propagation processes. The main findings are summarized as follows.

- The nucleation and propagation are induced by sequential gliding of Te atoms towards the center of the hexagon inside 2H structure. The barriers can be considerably reduced by the stress applied along armchair direction. By contrast, the stress applied along zigzag direction increases the barriers thus prohibits the nucleation and propagation.
- Under the stress on armchair direction, the nucleation is thermodynamically favorable through simultaneous transformation of multiple unit cells.
- Due to the non-symmetric phase boundaries, the direction of phase propagation is stress dependent and can be determined by the propagation barriers.
- The computed barriers imply that the phase transition of a pristine $MoTe_2$ is not kinetically favorable at room temperature even under a large stress. The defects inside $MoTe_2$ may play important roles in the phase transition.

Declaration of competing interest

The authors declare that they have no known competing financial interests or personal relationships that could have appeared to influence the work reported in this paper.

Acknowledgments

The authors gratefully acknowledge financial support of this work by the National Science Foundation, United States through Grant no. CMMI-1930783. This project was funded (in-part) by the University of Texas at San Antonio, United States, Office of the Vice President for Research, Economic Development & Knowledge Enterprise, United States. The authors thank Dr. Penghao Xiao, Dr. Joel Berry, and Dr. Tae Wook Heo from Lawrence Livermore National Laboratory for helpful discussions. The authors acknowledge the Texas Advanced Computing Center (TACC) at the University of Texas at Austin for providing HPC resources that have contributed to the research results reported within this paper.

References

[1] M. Wuttig, N. Yamada, Phase-change materials for rewriteable data storage, Nature Mater. 6 (11) (2007) 824–832, http://dx.doi.org/10.1038/nmat2009.
[2] Q. Wang, E.T. Rogers, B. Gholipour, C.M. Wang, G. Yuan, J. Teng, N.I. Zheludev, Optically reconfigurable metasurfaces and photonic devices based on phase change materials, Nature Photonics 10 (1) (2016) 60–65, http://dx.doi.org/10.1038/nphoton.2015.247.
[3] X. Qian, J. Liu, L. Fu, J. Li, Quantum spin hall effect in two - dimensional transition metal dichalcogenides, Science 346 (6215) (2014) 1344–1347, http://dx.doi.org/10.1126/science.1256815.
[4] K.-A.N. Duerloo, Y. Li, E.J. Reed, Structural phase transitions in two-dimensional Mo-and W-dichalcogenide monolayers, Nature Commun. 5 (2014) 4214.
[5] S. Song, D.H. Keum, S. Cho, D. Perello, Y. Kim, Y.H. Lee, Room temperature semiconductor-metal transition of MoTe2 thin films engineered by strain, Nano Lett. 16 (1) (2016) 188–193, http://dx.doi.org/10.1021/acs.nanolett.5b03481.
[6] Y. Wang, J. Xiao, H. Zhu, Y. Li, Y. Alsaid, K.Y. Fong, Y. Zhou, S. Wang, W. Shi, Y. Wang, A. Zettl, E.J. Reed, X. Zhang, Structural phase transition in monolayer MoTe2 driven by electrostatic doping, Nature 550 (7677) (2017) 487–491, http://dx.doi.org/10.1038/nature24043.
[7] Z. Dai, L. Liu, Z. Zhang, Strain engineering of 2D materials: Issues and opportunities at the interface, Adv. Mater. 31 (45) (2019) 1–11, http://dx.doi.org/10.1002/adma.201805417.
[8] W. Gao, R. Huang, Thermomechanics of monolayer graphene: Rippling, thermal expansion and elasticity, J. Mech. Phys. Solids 66 (1) (2014) 42–58, http://dx.doi.org/10.1016/j.jmps.2014.01.011.
[9] H.J. Conley, B. Wang, J.I. Ziegler, R.F. Haglund, S.T. Pantelides, K.I. Bolotin, Bandgap engineering of strained monolayer and bilayer MoS2, Nano Lett. (2013) http://dx.doi.org/10.1021/nl4014748, arXiv:1305.3880.
[10] Y.C. Lin, D.O. Dumcenco, Y.S. Huang, K. Suenaga, Atomic mechanism of the semiconducting-to-metallic phase transition in single-layered MoS 2, Nature Nanotechnol. 9 (5) (2014) 391–396, http://dx.doi.org/10.1038/nnano.2014.64.
[11] Y. Ma, B. Liu, A. Zhang, L. Chen, M. Fathi, C. Shen, A.N. Abbas, M. Ge, M. Mecklenburg, C. Zhou, Reversible semiconducting-to-metallic phase transition in chemical vapor deposition grown monolayer WSe2 and applications for devices, ACS Nano 9 (7) (2015) 7383–7391, http://dx.doi.org/10.1021/acsnano.5b02399.
[12] S. Cho, S. Kim, J.H. Kim, J. Zhao, J. Seok, D.H. Keum, J. Baik, D.H. Choe, K.J. Chang, K. Suenaga, S.W. Kim, Y.H. Lee, H. Yang, Phase patterning for ohmic homojunction contact in MoTe2, Science 349 (6248) (2015) 625–628, http://dx.doi.org/10.1126/science.aab3175.
[13] P. Zhang, L. Ma, F. Fan, Z. Zeng, C. Peng, P.E. Loya, Z. Liu, Y. Gong, J. Zhang, X. Zhang, P.M. Ajayan, T. Zhu, J. Lou, Fracture toughness of graphene, Nature Commun. 5 (2014) 3782, http://dx.doi.org/10.1038/ncomms4782.
[14] C. Lee, X. Wei, J.W. Kysar, J. Hone, Measurement of the elastic properties and intrinsic strength of monolayer graphene, Science 321 (5887) (2008) 385–388, http://dx.doi.org/10.1126/science.1157996.
[15] H. Zhu, Y. Wang, J. Xiao, M. Liu, S. Xiong, Z.J. Wong, Z. Ye, Y. Ye, X. Yin, X. Zhang, Observation of piezoelectricity in free-standing monolayer MoS2, Nature Nanotechnol. 10 (2) (2015) 151–155, http://dx.doi.org/10.1038/nnano.2014.309.
[16] S.P. Koenig, N.G. Boddeti, M.L. Dunn, J.S. Bunch, Ultrastrong adhesion of graphene membranes, Nature Nanotechnol. 6 (9) (2011) 543–546, http://dx.doi.org/10.1038/nnano.2011.123.
[17] Z. Cao, P. Wang, W. Gao, L. Tao, J.W. Suk, R.S. Ruoff, D. Akinwande, R. Huang, K.M. Liechti, A blister test for interfacial adhesion of large-scale transferred graphene, Carbon 69 (2014) 390–400, http://dx.doi.org/10.1016/j.carbon.2013.12.041.
[18] P. Wang, W. Gao, Z. Cao, K.M. Liechti, R. Huang, Numerical analysis of circular graphene bubbles, J. Appl. Mech. Trans. ASME 80 (4) (2013) http://dx.doi.org/10.1115/1.4024169.
[19] K. Yue, W. Gao, R. Huang, K.M. Liechti, Analytical methods for the mechanics of graphene bubbles, J. Appl. Phys. 112 (8) (2012) http://dx.doi.org/10.1063/1.4759146.
[20] W. Wu, L. Wang, Y. Li, F. Zhang, L. Lin, S. Niu, D. Chenet, X. Zhang, Y. Hao, T.F. Heinz, J. Hone, Z.L. Wang, Piezoelectricity of single-atomic-layer mos2 for energy conversion and piezotronics, Nature 514 (7253) (2014) 470–474, http://dx.doi.org/10.1038/nature13792.
[21] T. Jiang, R. Huang, Y. Zhu, Interfacial sliding and buckling of monolayer graphene on a stretchable substrate, Adv. Funct. Mater. 24 (3) (2014) 396–402, http://dx.doi.org/10.1002/adfm.201301999.
[22] W. Bao, F. Miao, Z. Chen, H. Zhang, W. Jang, C. Dames, C.N. Lau, Controlled ripple texturing of suspended graphene and ultrathin graphite membranes, Nature Nanotechnol. 4 (9) (2009) 562–566, http://dx.doi.org/10.1038/nnano.2009.191.

[23] H.H. Huang, X. Fan, D.J. Singh, H. Chen, Q. Jiang, W.T. Zheng, Controlling phase transition for single-layer MTe2 (M = Mo and W): Modulation of the potential barrier under strain, Phys. Chem. Chem. Phys. 18 (5) (2016) 4086–4094, http://dx.doi.org/10.1039/c5cp06706e.

[24] A. Krishnamoorthy, L. Bassman, R.K. Kalia, A. Nakano, F. Shimojo, P. Vashishta, Semiconductor-metal structural phase transformation in MoTe2 monolayers by electronic excitation, Nanoscale 10 (6) (2018) 2742–2747, http://dx.doi.org/10.1039/c7nr07890k.

[25] A. Ostadhossein, A. Rahnamoun, Y. Wang, P. Zhao, S. Zhang, V.H. Crespi, A.C. Van Duin, ReaxFF reactive force-field study of molybdenum disulfide (MoS2), J. Phys. Chem. Lett. 8 (3) (2017) 631–640, http://dx.doi.org/10.1021/acs.jpclett.6b02902.

[26] A. Ghasemi, P. Xiao, W. Gao, Nudged elastic band method for solid-solid transition under finite deformation, J. Chem. Phys. 151 (5) (2019) 54110, http://dx.doi.org/10.1063/1.5113716.

[27] A. Ghasemi, W. Gao, A method to predict energy barriers in stress modulated solid–solid phase transitions, J. Mech. Phys. Solids 137 (2020) http://dx.doi.org/10.1016/j.jmps.2019.103857.

[28] J. Berry, S. Zhou, J. Han, D.J. Srolovitz, M.P. Haataja, Dynamic phase engineering of bendable transition metal dichalcogenide monolayers, Nano Lett. 17 (4) (2017) 2473–2481, http://dx.doi.org/10.1021/acs.nanolett.7b00165.

[29] D. Pinchon, P.E. Hoggan, An introduction to transition state theory, J. Chem. Phys. 40 (7) (2007) 1597–1610, http://dx.doi.org/10.1063/1.4704546, arXiv:1602.06325.

[30] P. Hänggi, P. Talkner, M. Borkovec, Reaction-rate theory: Fifty years after Kramers, Rev. Modern Phys. 62 (2) (1990) 251–341, http://dx.doi.org/10.1103/RevModPhys.62.251.

[31] H. Jónsson, G. Mills, K.W. Jacobsen, Nudged elastic band method for finding minimum energy paths of transitions, in: Classical and Quantum Dynamics in Condensed Phase Simulations, World Scientific, 1998, pp. 385–404, http://dx.doi.org/10.1142/9789812839664_0016.

[32] D. Sheppard, P. Xiao, W. Chemelewski, D.D. Johnson, G. Henkelman, A generalized solid-state nudged elastic band method, J. Chem. Phys. 136 (7) (2012) 74103, http://dx.doi.org/10.1063/1.3684549.

[33] G. Kresse, J. Furthmüller, Efficient iterative schemes for ab initio total-energy calculations using a plane-wave basis set, Phys. Rev. B 54 (16) (1996) 11169–11186, http://dx.doi.org/10.1103/PhysRevB.54.11169.

[34] G. Kresse, Ab initio molecular dynamics for liquid metals, J. Non-Cryst. Solids 192–193 (1) (1995) 222–229, http://dx.doi.org/10.1016/0022-3093(95)00355-X.

[35] J.P. Perdew, K. Burke, M. Ernzerhof, Generalized gradient approximation made simple, Phys. Rev. Lett. 77 (18) (1996) 3865–3868, http://dx.doi.org/10.1103/PhysRevLett.77.3865.

[36] D. Joubert, From ultrasoft pseudopotentials to the projector augmented-wave method, Phys. Rev. B 59 (3) (1999) 1758–1775, http://dx.doi.org/10.1103/PhysRevB.59.1758.

[37] P.E. Blöchl, Projector augmented-wave method, Phys. Rev. B 50 (24) (1994) 17953.

[38] V.I. Levitas, H. Chen, L. Xiong, Triaxial-stress-induced homogeneous hysteresis-free first-order phase transformations with stable intermediate phases, Phys. Rev. Lett. 118 (2) (2017) http://dx.doi.org/10.1103/PhysRevLett.118.025701.

[39] Y. Li, K.A.N. Duerloo, K. Wauson, E.J. Reed, Structural semiconductor-to-semimetal phase transition in two-dimensional materials induced by electrostatic gating, Nature Commun. 7 (2016) 10671, http://dx.doi.org/10.1038/ncomms10671.

[40] V.I. Levitas, H. Chen, L. Xiong, Lattice instability during phase transformations under multiaxial stress: modified transformation work criterion, Phys. Rev. B 96 (5) (2017) 054118.

[41] H. Chen, V.I. Levitas, L. Xiong, Amorphization induced by 60° shuffle dislocation pileup against different grain boundaries in silicon bicrystal under shear, Acta Mater. 179 (2019) 287–295.

[42] Y. Peng, L. Xiong, Atomistic computational analysis of the loading orientation-dependent phase transformation in graphite under compression, JOM 71 (11) (2019) 3892–3902.

[43] K. Elibol, T. Susi, G. Argentero, M. Reza Ahmadpour Monazam, T.J. Pennycook, J.C. Meyer, J. Kotakoski, Atomic structure of intrinsic and electron-irradiation-induced defects in mote2, Chem. Mater. 30 (4) (2018) 1230–1238, http://dx.doi.org/10.1021/acs.chemmater.7b03760, arXiv:1802.01552.

[44] H. Zhu, Q. Wang, L. Cheng, R. Addou, J. Kim, M.J. Kim, R.M. Wallace, Defects and surface structural stability of mote2 under vacuum annealing, ACS Nano 11 (11) (2017) 11005–11014, http://dx.doi.org/10.1021/acsnano.7b04984.

[45] W. Zhou, X. Zou, S. Najmaei, Z. Liu, Y. Shi, J. Kong, J. Lou, P.M. Ajayan, B.I. Yakobson, J.C. Idrobo, Intrinsic structural defects in monolayer molybdenum disulfide, Nano Lett. 13 (6) (2013) 2615–2622, http://dx.doi.org/10.1021/nl4007479.

[46] J. Hong, Z. Hu, M. Probert, K. Li, D. Lv, X. Yang, L. Gu, N. Mao, Q. Feng, L. Xie, J. Zhang, D. Wu, Z. Zhang, C. Jin, W. Ji, X. Zhang, J. Yuan, Z. Zhang, Exploring atomic defects in molybdenum disulphide monolayers, Nature Commun. 6 (2015) 6293, http://dx.doi.org/10.1038/ncomms7293.